Inorganic Chemistry
Article
pubs.acs.org/IC

Photoconductivity in the Chalcohalide Semiconductor, SbSeI: a New Candidate for Hard Radiation Detection

Arief C. Wibowo,[†] Christos D. Malliakas,[†,‡] Zhifu Liu,[§] John. A. Peters,[§] Maria Sebastian,[§] Duck Young Chung,[†] Bruce W. Wessels,[§] and Mercouri G. Kanatzidis*[,†,‡]

[†]Materials Science Division, Argonne National Laboratory, Argonne, Illinois 60439, United States

[‡]Department of Chemistry and [§]Department of Materials Science and Engineering, Northwestern University, Evanston, Illinois 60208, United States

ABSTRACT: We investigated an antimony chalcohalide compound, SbSeI, as a potential semiconductor material for X-ray and γ-ray detection. SbSeI has a wide band gap of 1.70 eV with a density of 5.80 g/cm^3, and it crystallizes in the orthorhombic *Pnma* space group with a one-dimensional chain structure comprised of infinite zigzag chains of dimers $[Sb_2Se_4I_8]_n$ running along the crystallographic *b* axis. In this study, we investigate conditions for vertical Bridgman crystal growth using combinations of the peak temperature and temperature gradients as well as translation rate set in a three-zone furnace. SbSeI samples grown at 495 °C peak temperature and 19 °C/cm temperature gradient with 2.5 mm/h translation rate produced a single phase of columnar needlelike crystals aligned along the translational direction of the growth. The ingot sample exhibited an n-type semiconductor with resistivity of ~10^8 Ω·cm. Photoconductivity measurements on these specimens allowed us to determine mobility−lifetime ($\mu\tau$) products for electron and hole carriers that were found to be of similar order of magnitude (~10^{-4} cm^2/V). Further, the SbSeI ingot with well-aligned, one-dimensional columnar needlelike crystals shows an appreciable response of Ag Kα X-ray.

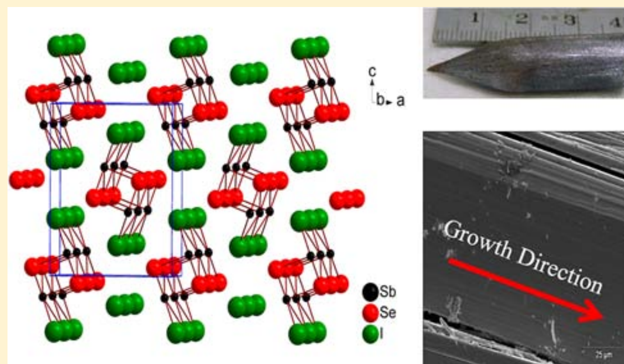

■ INTRODUCTION

New demands in hard radiation (such as X-rays and γ-rays) detection for the purposes of homeland security, biomedical and dental diagnostics, as well as other scientific applications require high-efficiency devices. Semiconductors with wide band gaps and high mass densities are promising all-solid-state radiation detector materials for room temperature applications.[1] Currently, the leading semiconductors under investigation are compounds such as $Cd_{1-x}Zn_xTe$ (CZT) and TlBr. These materials have undergone nearly 4 decades of development, and CZT has reached a mobility-lifetime ($\mu\tau$) product for electrons of ~10^{-2} cm^2/V with energy resolution of near 2% at 662 keV, while TlBr has a $\mu\tau$ product for electrons of ~10^{-3} cm^2/V and energy resolution of ~2.4%.[2] The two systems, however, have drawbacks. High-performance CZT comes in low yield, has compositional nonuniformity, and exhibits much lower $\mu\tau$ products for holes.[3] TlBr is subject to polarization-induced instability at room temperature operation.[4]

The ultimate goal for high-resolution γ-ray detectors is to have a material with near-perfect charge-transport properties similar to cryogenically cooled germanium but capable of operating at room temperature. This can be achieved with semiconducting crystals having high $\mu\tau$ products for both electrons and holes and extremely low concentrations of electrically active and carrier-trapping defects. A single crystal with high-dimensional structure and low defect concentration is typically pursued. Recent efforts, however, indicate that a well-aligned polycrystalline thick film can also reach ideal single-crystal properties with the advantage of large area imaging sensors.[5] We are interested in exploring the potential of inorganic chalcohalide crystals as potential hard radiation detection materials for room temperature application.

A combination of properties, i.e., high-density structure with high atomic number and simultaneously a wide band gap (e.g., >1.6 eV), are required for a single, ideal compound for X-ray and γ-ray detection. Heavy-atom-containing chalcogenides possess high-density and semiconducting properties but often have narrow band gaps, which lead to a large dark current. Heavy-element-containing binary halides, on the other hand, can be reactive and tend to have band gaps that are too large, which suppresses the photoexcited carrier mobility. Herein, we introduce hybrid ternary, crystalline chalcohalides as potential candidates for semiconductor radiation detectors. The importance of the class of chalcohalide crystalline compounds is often overlooked compared to the glass ones because the latter are well-known for their mid-IR optics and ionic superconductivity properties,[6] and yet several unique functional properties of crystalline chalcohalide compounds have been reported, which include X-ray and γ-ray detection material,[7]

Received: March 4, 2013
Published: May 28, 2013

ACS Publications © 2013 American Chemical Society

dx.doi.org/10.1021/ic401086r | Inorg. Chem. 2013, 52, 7045−7050

ferroelectricity,[8] optical nonlinearity,[9] upconversion luminescence,[10] and phase transitions.[11]

Chalcohalide, a hybrid compound that introduces halogen atoms into the chalcogenide framework structure, disrupts the extensive orbital overlap of the chalcogenide, and a widening of the band gap toward the desired range for X-ray and γ-ray detection (1.6 to ~2.5 eV) is anticipated. In addition, the chemical robustness of chalcogenides can be imparted in the hybrid chalcohalides. We investigate high atomic number, such as bismuth and antimony, ternary chalcohalides and selected three potential candidates (BiSBr,[12] SbSBr,[13] and SbSeI[14]) that belong to the chalcohalide families, MQX, all with a one-dimensional overall structure. The materials meet the immediate physical property requirements, namely, density and band gap for γ-ray detector materials. BiSBr (band gap ~1.95 eV and density 6.57 g/cm^3) and SbSBr (band gap ~2.20 eV and density 4.97 g/cm^3) were found to be incongruently melting; therefore, we have concentrated our crystal growth attempts on SbSeI (band gap ~1.70 eV and density 5.80 g/cm^3) because it remains intact after several Bridgman growth runs.

Here we present our results on antimony-based ternary chalcohalide, SbSeI, and assess its potential in terms of crystal growth, thermal behavior, electrical resistivity, charge carrier type, and mobility−lifetime ($\mu\tau$) products, as well as Ag Kα X-ray response. An important finding in this report is that, despite the polycrystalline but well-aligned nature of the SbSeI ingot, we can still observe the photoconductivity response to X-ray radiation.

■ EXPERIMENTAL SECTION

Synthesis. SbI_3 (99.999%, Alfa Aesar), antimony (Sb; 99.999%, CERAC), and selenium (Se; 99.999%, Alfa Aesar) were used as starting materials without further purification. All manipulations were carried out in a glovebox under a N_2 atmosphere.

Stoichiometric amounts of SbI_3, Sb, and Se with a total mass of 10 g were ground and loaded into a 15 mm outer diameter (O.D.) × 12 mm i.d. × 30 cm length fused silica tube and subsequently sealed under a $<10^{-4}$ mbar vacuum. The reaction mixture was placed in a programmable tube furnace, and the temperature was raised to 500 °C over 16 h, dwelling there for 2 days with 2 h of rocking to ensure homogeneous mixing of the melt, followed by cooling to room temperature over 6 h.

Crystal Growth and Sample Preparations. The obtained pure polycrystalline material was then sealed under a $<10^{-4}$ mbar vacuum in a 12 mm O.D. × 9 mm i.d. × 20 cm length fused silica ampule with a tapered end and premelted in a box furnace prior to crystal growth in a vertical Bridgman furnace with three 20-cm-long heating zones. The resulting premelted ingot filled about one-fourth of the ampule length. Several attempts for crystal growth were performed using combinations of the peak temperature and temperature gradient set in the furnace and the translation rate of the material through the heating zones. We observed that running a sample at 560 °C peak temperature with a 28 °C/cm temperature gradient and a 2.5 mm/h translation rate decomposed SbSeI into SbI_3 and Sb_2Se_3. Rerunning the same sample under the same conditions broke the ampule because of overpressure from SbI_3. The peak temperature of around 500 °C was set to avoid formation of SbI_3. The growth condition, which provided the best quality ingot from the conditions that we attempted, was a combination of 495 °C peak temperature, 19 °C/cm temperature gradient, and 2.5 mm/h translation rate.

The ingot obtained was 4 cm length × 9 mm diameter with dark-red SbSeI needles grown parallel along the crystallographic *b* axis (the translational direction of the growth). The ingot was embedded in epoxy and sliced to 3-mm-thick disks using a precision saw (Struers Secotom 50). The coin-shape disk sample embedded in epoxy was then very carefully hand polished using SiC sandpaper with grits of P280, P1200, and P4000 in this order. The resistivity and photoconductivity measurements were conducted on these types of samples.

Scanning Electron Microscopy (SEM). The cross section of the ingot was examined under a Hitachi SEM 3400 scanning electron microscope equipped with an Oxford Instruments energy-dispersive spectroscopy detector. Data were acquired with an accelerating voltage of 20 keV and in 60 s accumulation time.

Powder X-ray Diffraction (PXRD). In order to examine the phase purity of the samples, a small portion was obtained from three different locations along the length of the ingot. The ground powder of three samples taken from the tip (1), the middle (2), and the top of the ingot (3) was used to collect PXRD patterns using a PanAlytical X'Pert Pro powder diffractometer (Cu Kα radiation λ = 1.5418 Å) over the 2θ range of 10−70°, with a step size of 0.02° and a scan speed of 0.25°/min.

UV−Visible Spectroscopy. Optical diffuse-reflectance measurements were performed at room temperature using a Shimadzu UV-3600 spectrophotometer operating in the 200−2500 nm region. The instrument is equipped with an integrating sphere and controlled by a personal computer. $BaSO_4$ was used as a 100% reflectance standard. The sample was prepared by grinding the cut ingot and spreading it on a compacted surface of the powdered standard material preloaded into a sample holder. The reflectance versus wavelength data generated were used to estimate the band gap of the material by converting reflectance to absorption data according to the Kubelka−Munk equation $\alpha/S = (1 - R)^2/2R$, where R is the reflectance and α and S are the absorption and scattering coefficients, respectively.[15]

Differential Thermal Analysis (DTA). Experiments were performed on a Shimadzu DTA-50 thermal analyzer. A sample (~30 mg) of ground crystalline material was sealed in a silica ampule under vacuum. An ampule of equal mass filled with Al_2O_3 was sealed and placed on the reference side of the detector. The sample was heated to 500 °C at 5 °C/min, and after 10 min, it was cooled at a rate of −5 °C/min to 50 °C. Three cycles of heating and cooling were conducted on the sample. The melting and crystallization points were measured at the onset of the endothermic and exothermic peaks. The residues of the DTA experiments were examined by PXRD.

Electrical Properties, Photoconductivity Measurements, and Detection Properties. Direct-current (dc) conductivity was measured with a Keithley model 617 electrometer using graphite paste as a conducting material for SbSeI to establish a good ohmic contact (silver paste is not suitable because of a side reaction with SbSeI). Electrical resistivities as a function of the temperature and room temperature Seebeck coefficient were measured by a Keithley model 2182A nanovoltmeter and a 6514 electrometer under vacuum. The electrical resistivity was measured from room temperature to 500 K, which was controlled by a K-20 temperature controller of MMR Technologies, Inc. The dimension of a block sample measured was 0.4 × 1.3 × 2.0 mm^3. The photoconductivity was measured using a custom setup, as described previously.[7,16] A helium−neon laser (633 nm) chopped at 465 Hz was focused on the surface of the sample. The output photocurrent signal was collected as the voltage drop on a load resistance R (5 kΩ) and analyzed by the lock-in amplifier. Graphite electrodes were pasted on the front and back surfaces of a sample in a parallel-plate configuration. The $\mu\tau$ products for electrons and holes were obtained by applying either negative or positive voltage to the illuminated electrode and by measuring the photocurrent for electrons and holes. A qualitative measurement of Ag Kα X-ray detection was conducted using a custom-made setup. A disk sample with dimensions of 3 mm thickness × 9 mm diameter was put inside a guarded box with a copper wire and graphite paste used as the contact. The sample was irradiated by Ag Kα X-ray (22.15 keV, 0.559 Å) with an ON−OFF state, along the direction of the sample thickness (growth direction of well-aligned crystals). This was repeated four times, with different applied voltage biases (5, 50, and 100 V). The resulting photocurrent was recorded as a function of time.

RESULTS AND DISCUSSION

Synthesis, Crystal Growth, and Sample Preparation. Single-phase, polycrystalline SbSeI was obtained from the reaction of a stoichiometric mixture of SbI_3, Sb, and Se at 500 °C in a closed quartz ampule. SbSeI crystallizes in an orthorhombic crystal system with the *Pnma* space group [a = 8.698(2) Å, b = 4.127(1) Å, and c = 10.412(2) Å], and it has a one-dimensional chain structure comprised of infinite zigzag dimers of $[Sb_2Se_4I_8]_n$ square pyramids along the crystallographic b axis. The parallel chains are linked to one another by the weaker bonding of Sb−I [bond distance of 3.823(1) Å], as shown in Figure 1.[17] Prior to crystal growth, the thermal

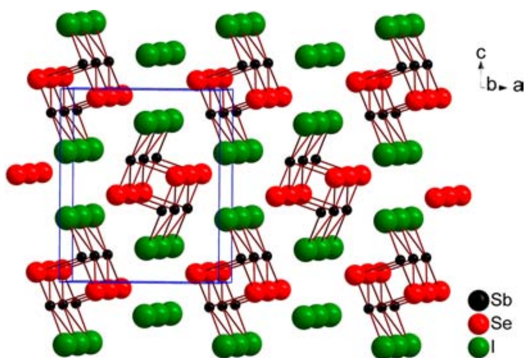

Figure 1. Structure of SbSeI crystallized in the *Pnma* space group with the unit cell parameters of a = 8.698(2) Å, b = 4.127(1) Å, and c = 10.412(2) Å.[17]

behavior and melting and crystallization temperatures of SbSeI were examined by DTA. After three cycles of heating and cooling, a constant endothermic peak at 453 °C (melting point) and exothermic peak at 410 °C (crystallization point) with no other thermal events were observed, and the temperature profiles for Bridgman crystal growth was constructed based on this result.

Several growth attempts using a three-zone vertical furnace were conducted to optimize the growth conditions for obtaining a high-quality ingot with the least physical defects and high directionality of SbSeI needles along the growth direction. Such attempts involved variations of the following combinations: (a) peak temperature (495 and 560 °C), (b) temperature gradient (19 and 28 °C/cm) defined as the slope of temperature over the length of the heating zone between melting and crystallization temperatures, and (c) translation rate defined as the speed of the sample translating down through the furnace (5 and 2.5 mm/h). The condition that produced the best quality ingot was a combination of 495 °C peak temperature, 19 °C/cm temperature gradient, and 2.5 mm/h translation rate. The temperature profile for this condition is shown in Figure 2.

The phase purity of the resulting SbSeI ingot was evaluated using PXRD. The diffraction patterns of three separate specimens that were obtained from different locations along the ingot (sample 1 was from the tip of the ingot, 2 from the middle, and 3 from the top, as shown in Figure 3) matched the simulated patterns based on the single-crystal structure. This demonstrates that all samples used for further optical and electrical properties and photoconductivity measurements were of single-phase quality.

A photograph of an ingot of SbSeI with 4 cm length × 9 mm diameter after Bridgman growth using the appropriate

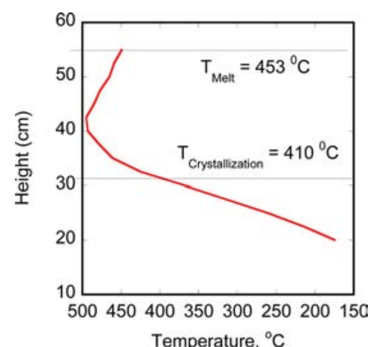

Figure 2. Temperature profile of a three-zone vertical Bridgman furnace used to grow SbSeI.

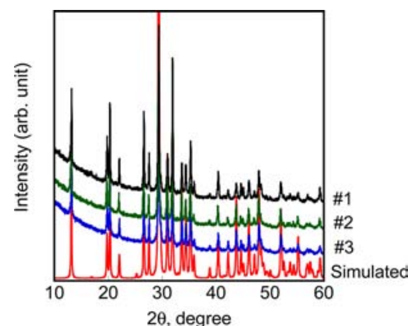

Figure 3. PXRD patterns (Cu Kα radiation) of samples obtained from different locations of the SbSeI crystal ingot.

conditions mentioned above shows the needlelike character of the SbSeI crystals oriented along the growth direction (Figure 4A). The optical micrograph of the cross section of the

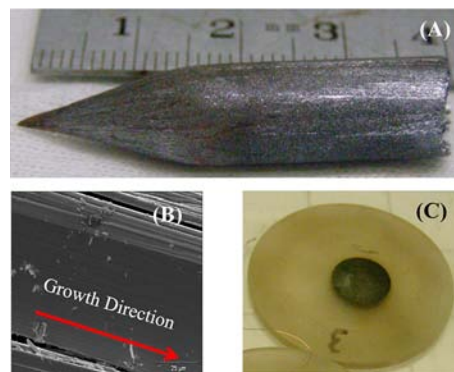

Figure 4. (A) Typical image of an ingot obtained from vertical Bridgman growth. (B) SEM image of SbSeI showing long crystals grown along the translational direction of vertical Bridgman growth. (C) SbSeI sample embedded in epoxy, cut, and hand polished for property measurements.

SbSeI ingot shows needlelike crystals grown along the translational direction of the Bridgman growth (Figure 4B). Sample preparation for characterization of grown SbSeI requires special care because of the intrinsic fragile nature of the needlelike crystal ingot. Embedding the sample in epoxy with cutting and hand polishing was proven effective in preventing sample fracture. Figure 4C shows the SbSeI ingot embedded in epoxy, cut with 3 mm thickness, and hand polished.

dx.doi.org/10.1021/ic401086r | Inorg. Chem. 2013, 52, 7045−7050

Thermal Properties. The thermal behavior of SbSeI was investigated by three consecutive cycles of heating and cooling at DTA. The compound exhibits a sharp endothermic peak upon heating (melting point at 453 °C) and a sharp exothermic peak upon cooling (crystallization point at 410 °C) throughout the three consecutive cycles (Figure 5). This indicates congruent melting of the compound within the limit of the experiment. The PXRD pattern of the sample after DTA measurements showed that the SbSeI compound is still intact with no sign of decomposition.

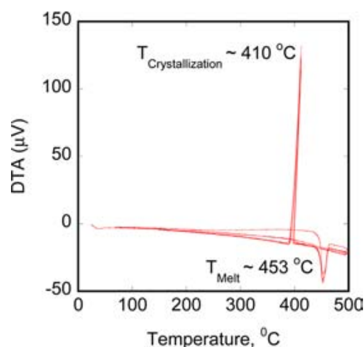

Figure 5. DTA thermogram of three consecutive heating and cooling cycles of SbSeI at a rate of 5 °C/min.

We observed, however, that decomposition of SbSeI into SbI_3 and Sb_2Se_3 occurred when it was exposed to a Bridgman growth condition at 560 °C peak temperature with 28 °C/cm temperature gradient and 2.5 mm/h translation rate. This particular condition allows decomposition of SbSeI and separation of volatile SbI_3 to the cold part of the ampule, indicating that SbSeI decomposes at a temperature well beyond its melting point. Because of this, the peak temperature in our crystal growth condition was set to around 500 °C and produced good-quality ingots with no sign of decomposition.

Optical Properties. The electronic absorption spectra obtained from diffuse-reflectance spectra at room temperature show that SbSeI has an indirect band gap of ~1.70 eV (Figure 6), which is consistent with the dark-red crystals and in agreement with the previously reported value.[14,18] Several band structure calculations for the room temperature paraelectric phase of SbSeI have been reported based on density functional theory[19] and based on an empirical pseudopotential method.[14b] The former study predicts an indirect band gap of 1.65 eV, in which the maximum of the valence band and the minimum of the conduction band are located at the Γ and S symmetry points at the Brillouin zone, respectively. The latter calculations estimated an indirect band gap of 1.67 eV. Other theoretical reports suggest an indirect band gap of 1.71 eV[20] for SbSeI at room temperature.

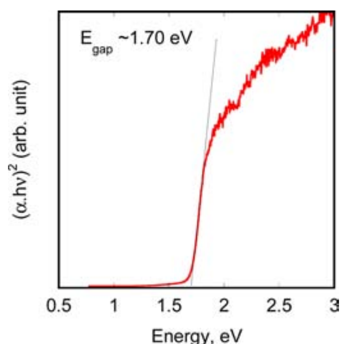

Figure 6. Optical absorption spectrum of SbSeI showing an indirect band gap of ~1.70 eV at room temperature.

Electrical Properties, Photoconductivity Measurements, and Detection Properties. The room temperature electrical resistivity of our SbSeI specimens was on the order of 10^8 Ω·cm, and this value is consistent with the literature.[21] From room temperature measurements of the Seebeck coefficient as well as electrical resistivity measurement as a function of the temperature, we found that our SbSeI samples are n-type semiconductors at room temperature and exhibit an increase in the electrical conductivity with increasing temperature (Figure 7), consistent with semiconducting behavior.

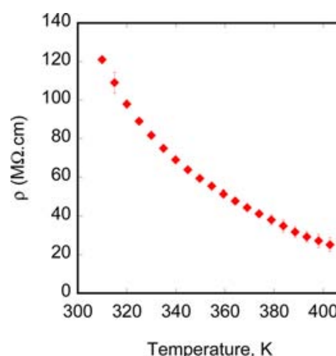

Figure 7. Electrical resistivity of a SbSeI single-crystal sample as a function of the temperature.

Photoconductivity measurements to obtain $\mu\tau$ products were conducted on suitably cut and polished disk samples with 9 mm diameter and 3 mm thickness. Different voltage polarities were applied to the illuminated sample. The resulting voltage dependence of the photocurrent can be modeled as

$$I(V) = \frac{I_0 \mu\tau V}{L^2} \frac{1 - e^{-L^2/\mu\tau V}}{1 + \frac{L}{V}\frac{s}{\mu}} \qquad (1)$$

for strongly absorbed light, where I_0 is the saturation current, L is the sample thickness, s is the surface recombination velocity, and V is the applied voltage.[22] The representative photoconductivity curves are shown in Figure 8. The estimated $\mu\tau$ products for electrons and holes are 4.41×10^{-4} and 3.52×10^{-4} cm²/V, respectively.

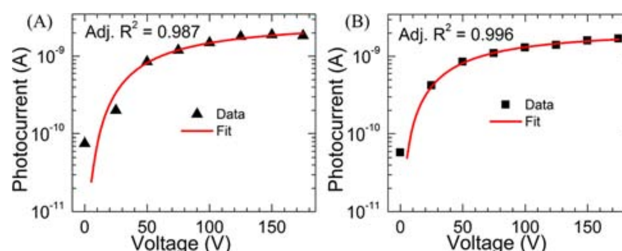

Figure 8. Photocurrent as a function of the applied voltage for electrons (A) and holes (B) measured on a SbSeI disk. The $\mu\tau$ products are 4.41×10^{-4} and 3.52×10^{-4} cm²/V for electrons and holes, respectively.

The observed $\mu\tau$ products are high enough to make SbSeI a potentially interesting detector material, and this assessment is strengthened by the very similar magnitudes for electrons and holes, i.e., $\sim10^{-4}$ cm^2/V. The latter indicates that the amounts of charge carriers collected are similar for both electrons and holes, which would be very beneficial for detector design. In contrast, commercially available CZT has a low $\mu\tau$ product for holes compared to that of electrons; therefore, a so-called single-carrier-detector[23] design is utilized, where only one type of charge carrier (electrons in the CZT case) is collected and read.

The observed $\mu\tau$ products for the SbSeI samples are comparable to the leading semiconductor detector materials at present, such as CZT,[2a] TlBr,[2c,4] $Cs_2Hg_6S_7$,[16d] Tl_6SeI_4,[7] and α-HgI_2[24] (Table 1). Unlike the leading semiconductor detector materials, which typically contain higher-dimensional single crystals, SbSeI with well-aligned, one-dimensional, columnar needlelike crystals still shows promise for hard radiation detection.

Table 1. Mobility−Lifetime ($\mu\tau$) Products of SbSeI Compared to the Current Leading Semiconductors in γ-ray Detector Applications

compound	structure dimension	$(\mu\tau)_e$ (cm^2/V)	$(\mu\tau)_h$ (cm^2/V)	ref
CZT	3D	2.30×10^{-2}	2.40×10^{-5}	2a
TlBr	3D	6.50×10^{-3}	$\sim10^{-4}$	2c, 4
$Cs_2Hg_6S_7$	3D	1.20×10^{-3}	1.00×10^{-4}	16d
Tl_6SeI_4	3D	7.00×10^{-3}	6.00×10^{-4}	7
α-HgI_2	2D	8.00×10^{-4}	3.00×10^{-5}	24
SbSeI	1D	4.41×10^{-4}	3.52×10^{-4}	this work

Upon exposure to Ag Kα X-rays, the SbSeI samples show an appreciable response in terms of observed photocurrent as function of time under 5, 50, and 100 V applied biases. Four cycles of the ON−OFF X-ray beam state show consistent behavior without any indication of degradation in all three applied biases (Figure 9). Upon switching off the X-ray beam, the photocurrent decays slowly and recovery to the dark condition requires a few minutes. This long-tail photocurrent decay indicates a slow thermal release of charge carriers from deep trap states, and subsequent recombination takes place.[25] The absolute photocurrent value increases as the applied bias increases, consistent with the good photoconductivity properties of SbSeI.

Considering that all chemicals used in this SbSeI crystal growth were utilized without further purification, and the relatively fast translation rates (2.5 mm/h) used for crystal growth, the observed $\mu\tau$ products are respectably high. Better purification processes combined with further optimized crystal growth conditions may yield even higher $\mu\tau$ products and resistivity in SbSeI samples and, hence, may give better hard radiation detection properties.

■ CONCLUSIONS

Our efforts to identify high-performance X-ray and γ-ray semiconductor detector materials under the concept of hybridizing wide-band-gap halides with narrow-band-gap chalcogenides, led to SbSeI as a promising semiconductor. Other chalcohalides investigated, BiSBr and SbSBr, were found to be incongruent melting during vertical Bridgman growth and, hence, complicating their crystal growth. Our preliminary crystal growth experiments of SbSeI using a vertical Bridgman method produced a single-phase ingot with SbSeI needlelike crystals aligned in the translational direction of the growth. The sample from this ingot shows the highest values of resistivity ($\sim10^8$ Ω·cm), n-type conductivity, and promising $\mu\tau$ products of $\sim10^{-4}$ cm^2/V for both electrons and holes. In addition, we observed an appreciable Ag Kα X-ray photocurrent response. Despite its one-dimensional, columnar needlelike crystal morphology, SbSeI is a semiconductor with potential for hard radiation detection comparable to its higher dimensional, single-crystal counterparts. Improved growth conditions of this inorganic compound are expected to give samples with even greater hard radiation response.

■ AUTHOR INFORMATION

Corresponding Author

*E-mail: m-kanatzidis@northwestern.edu.

Author Contributions

The manuscript was written through contributions of all authors. All authors have given approval to the final version of the manuscript.

Notes

The authors declare no competing financial interest.

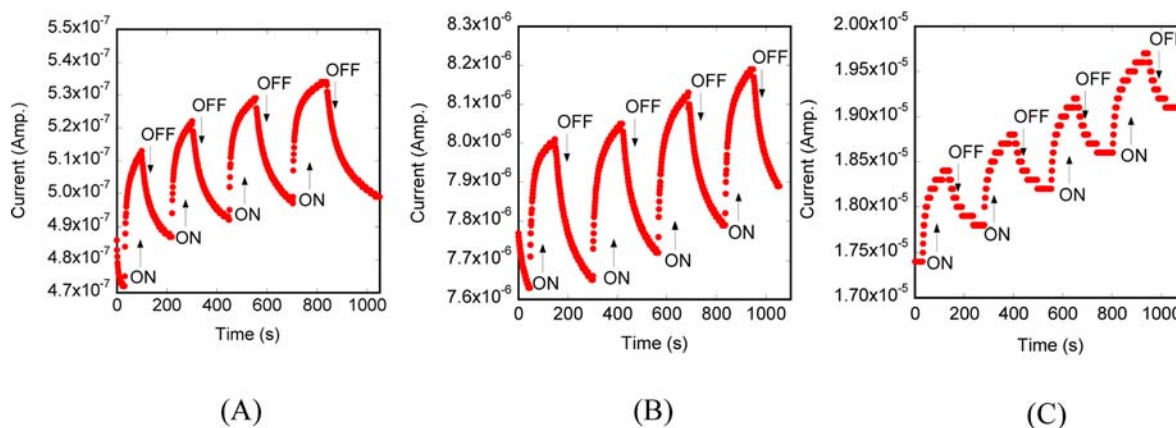

Figure 9. SbSeI detection of Ag Kα radiation with repeated ON−OFF switching of the X-ray beam under different applied biases: (A) 5 V; (B) 50 V; (C) 100 V.

dx.doi.org/10.1021/ic401086r | Inorg. Chem. 2013, 52, 7045−7050

■ ACKNOWLEDGMENTS

This work was supported by the Office of Nonproliferation and Verification Research and Development under National Nuclear Security Administration of the U.S. Department of Energy under Contract DE-AC02-06CH11357. The work in Northwestern University (by B.W.W.) was supported by the Defense Threat Reduction Agency through Grant HDTRA1 09-1-0044.

■ REFERENCES

(1) (a) Fano, U. *Phys. Rev.* **1946**, *70*, 44. (b) Fano, U. *Phys. Rev.* **1947**, *72*, 26.
(2) (a) Amman, M.; Lee, J. S.; Luke, P. N.; Chen, H.; Awadalla, S. A.; Redden, R.; Bindley, G. *IEEE Trans. Nucl. Sci.* **2009**, *56*, 795. (b) Kim, H.; Churilov, A.; Ciampi, G.; Cirignano, L.; Higgins, W.; Kim, S.; O'Dougherty, P.; Olschner, F.; Shah, K. *Nucl. Instrum. Methods Phys. Res., Sect. A* **2011**, *629*, 192. (c) Kim, H.; Kargar, A.; Cirignano, L.; Churilov, A.; Ciampi, G.; Higgins, W.; Olschner, F.; Shah, K. *IEEE Trans. Nucl. Sci.* **2012**, *59*, 243.
(3) Bolotnikov, A. E.; Camarda, G. S.; Cui, Y.; Hossain, A.; Yang, G.; Yao, H. W.; James, R. B. *IEEE Trans. Nucl. Sci.* **2009**, *56*, 791.
(4) Hitomi, K.; Matsumoto, M.; Muroi, O.; Shoji, T.; Hiratate, Y. *IEEE Trans. Nucl. Sci.* **2002**, *49*, 2526.
(5) Sellin, P. J. *Nucl. Instrum. Methods Phys. Res., Sect. A* **2006**, *563*, 1.
(6) (a) Bychkov, E. *Solid State Ionics* **2009**, *180*, 510. (b) Fuxi, G. *J. Non-Cryst. Solids* **1992**, *140*, 184.
(7) Johnsen, S.; Liu, Z.; Peters, J. A.; Song, J.-H.; Nguyen, S.; Malliakas, C. D.; Jin, H.; Freeman, A. J.; Wessels, B. W.; Kanatzidis, M. G. *J. Am. Chem. Soc.* **2011**, *133*, 10030.
(8) (a) Itoh, K.; Matsunaga, H.; Nakamura, E. *J. Phys. Soc. Jpn.* **1976**, *41*, 1679. (b) Xu, Z. C.; Fong, C. Y.; Wooten, F.; Yeh, Y. *Ferroelectrics* **1984**, *56*, 187.
(9) (a) Cai, Y.; Wang, Y.; Li, Y.; Wang, X.; Xin, X.; Liu, C.; Zheng, H. *Inorg. Chem.* **2005**, *44*, 9128. (b) Guo, S.-P.; Guo, G.-C.; Wang, M.-S.; Zou, J.-P.; Zeng, H.-Y.; Cai, L.-Z.; Huang, J.-S. *Chem. Commun.* **2009**, 4366. (c) Zhang, Q.; Chung, I.; Jang, J. I.; Ketterson, J. B.; Kanatzidis, M. G. *J. Am. Chem. Soc.* **2009**, *131*, 9896.
(10) (a) Xu, Y.; Chen, D.; Zhang, Q.; Zeng, H.; Shen, C.; Adam, J.-l.; Zhang, X.; Chen, G. *J. Phys. Chem. C* **2009**, *113*, 9911. (b) Wang, W.; Zhang, Q.; Xu, Y.; Shen, C.; Chen, D.; Chen, G. *J. Am. Ceram. Soc.* **2010**, *93*, 2445.
(11) (a) Nilges, T.; Osters, O.; Bawohl, M.; Bobet, J.-L.; Chevalier, B.; Decourt, R.; Weihrich, R. *Chem. Mater.* **2010**, *22*, 2946. (b) Kong, S.-T.; Deiseroth, H.-J.; Reiner, C.; Gun, O.; Neumann, E.; Ritter, C.; Zahn, D. *Chem.—Eur. J.* **2010**, *16*, 2198. (c) Gagor, A.; Pietraszko, A.; Kaynts, D. *J. Solid State Chem.* **2005**, *178*, 3366.
(12) (a) Arivuoli, D.; Gnanam, F. D.; Ramasamy, P. *J. Phys. D: Appl. Phys.* **1988**, *21*, 1019. (b) Oppermann, H.; Petasch, U. *Z. Naturforsch., B: J. Chem. Sci.* **2003**, *58*, 725.
(13) Jin, M.-S.; Park, K.-H.; Kim, H.-G.; Choe, S.-H.; Park, B.-S.; Hyun, S.-C.; Kim, W.-T. *Semicond. Sci. Technol.* **1995**, *10*, 1167.
(14) (a) Aliev, Z. S.; Musaeva, S. S.; Babanly, D. M.; Shevelkov, A. V.; Babanly, M. B. *J. Alloys Compd.* **2010**, *505*, 450. (b) Alward, J. F.; Fong, C. Y.; El-Batanouny, M.; Wooten, F. *Solid State Commun.* **1978**, *25*, 307.
(15) (a) Morris, C. D.; Kanatzidis, M. G. *Inorg. Chem.* **2010**, *49*, 9049. (b) Kortum, G.; Braun, W.; Herzog, G. *Angew. Chem.* **1963**, *75*, 653. (c) Larson, P.; Mahanti, S. D.; Kanatzidis, M. G. *Phys. Rev. B* **2000**, *61*, 8162. (d) McCarthy, T. J.; Tanzer, T. A.; Kanatzidis, M. G. *J. Am. Chem. Soc.* **1995**, *117*, 1294. (e) Trikalitis, P. N.; Rangan, K. K.; Bakas, T.; Kanatzidis, M. G. *J. Am. Chem. Soc.* **2002**, *124*, 12255.
(16) (a) Li, H.; Malliakas, C. D.; Liu, Z.; Peters, J. A.; Jin, H.; Morris, C. D.; Zhao, L.; Wessels, B. W.; Freeman, A. J.; Kanatzidis, M. G. *Chem. Mater.* **2012**, *24*, 4434. (b) Li, H.; Peters, J. A.; Liu, Z.; Sebastian, M.; Malliakas, C. D.; Androulakis, J.; Zhao, L.; Chung, I.; Nguyen, S.; Johnsen, S.; Wessels, B. W.; Kanatzidis, M. G. *Cryst. Growth Des.* **2012**, *12*, 3250. (c) Liu, Z.; Peters, J. A.; Wessels, B. W.; Johnsen, S.; Kanatzidis, M. G. *Nucl. Instrum. Methods Phys. Res., Sect. A* **2011**, *659*, 333. (d) Androulakis, J.; Peter, S. C.; Li, H.; Malliakas, C. D.; Peters, J. A.; Liu, Z.; Wessels, B. W.; Song, J.-H.; Jin, H.; Freeman, A. J.; Kanatzidis, M. G. *Adv. Mater.* **2011**, *23*, 4163. (e) Johnsen, S.; Liu, Z.; Peters, J. A.; Song, J.-H.; Peter, S. C.; Malliakas, C. D.; Cho, N. K.; Jin, H.; Freeman, A. J.; Wessels, B. W.; Kanatzidis, M. G. *Chem. Mater.* **2011**, *23*, 3120.
(17) (a) Voutsas, G. P.; Rentzeperis, P. J. *Z. Kristallogr.* **1982**, *161*, 111. (b) Ibanez, A.; Jumas, J. C.; Fourcade, J. O.; Philippot, E.; Maurin, M. *J. Solid State Chem.* **1983**, *48*, 272.
(18) (a) Park, S.-A.; Kim, M.-Y.; Lim, J.-Y.; Park, B.-S.; Koh, J.-D.; Kim, W.-T. *Phys. Status Solidi B* **1995**, *187*, 253. (b) Shin, D.-W.; Hyeun, S.-C.; Park, S.-A.; Kim, Y.-G.; Kim, C.-D.; Kim, W.-T. *J. Phys. Chem. Solids* **1994**, *55*, 825.
(19) Akkus, H.; Kazempour, A.; Akbarzadeh, H.; Mamedov, A. M. *Phys. Status Solidi B* **2007**, *244*, 3673.
(20) Pikka, T. A.; Fridkin, V. M. *Fiz. Tverd. Tela* **1969**, *10*, 2668.
(21) Chepur, D. V.; Bercha, D. M.; Turyanitsa, I. D.; Slivka, V. Y. *Phys. Status Solidi B* **1968**, *30*, 461.
(22) Many, A. *J. Phys. Chem. Solids* **1965**, *26*, 575.
(23) Luke, P. N.; Amman, M. *IEEE Trans. Nucl. Sci.* **2007**, *54*, 834.
(24) (a) Owens, A. J. *J. Synchrotron Radiat.* **2006**, *13*, 143. (b) Kargar, A.; Ariesanti, E.; McGregor, D. S. *Nucl. Technol.* **2011**, *175*, 131.
(25) Gupta, D.; Brenner, T. J. K.; Albert-Seifried, S.; Lee, M. J.; Heeney, M.; McCulloch, I.; Sirringhaus, H. *Org. Electron.* **2012**, *13*, 36.